Monatshefte für Chemie - Chemical Monthly (2022) 153:597–607
https://doi.org/10.1007/s00706-022-02955-3

ORIGINAL PAPER

Adsorption, photodegradation, and selective removal of reactive red 2 dye onto cuprous oxide nanoparticles

Ahmed F. Halbus[1] · Zahraa H. Athab[2] · Ahmed S. Abbas[1] · Ahmed K. Khaleel[1] · Suhailah M. Wahhoodee[1] · Abbas J. Atiyah[1]

Received: 7 April 2022 / Accepted: 27 June 2022 / Published online: 18 July 2022

Abstract

Environmentally friendly nanoparticles are often utilized to remediate organic pollutants such as dyes in water bodies. Herein, we describe the adsorption and photocatalytic properties of Cu_2O nanoparticles (Cu_2ONPs) for the removal of reactive red 2 dye (RR2) from synthetic dye solutions. Cu_2ONPs as an adsorbent is synthesized by direct precipitation method using sodium hydroxide with cupric chloride in the existence of ascorbic acid as a reducing agent. Scanning electron microscopy (SEM), X-ray diffraction (XRD), dynamic light scattering (DLS) and Fourier transform infrared (FT-IR) analysis were used to characterize the synthesized Cu_2ONPs. SEM images show that the average size as-prepared of Cu_2ONPs was determined to be 62.84 ± 11 nm with a homogenous cubic shape. The zeta potential of NPs was measured to be $+22 \pm 5$ mV with a hydrodynamic diameter of 147 ± 8 nm, according to DLS results. The nanoparticles exhibit excellent adsorption activity for RR2 solution (10–60 μg cm^{-3}) at room temperature and pH 5. The RR2 dye adsorption on nanoparticles in the existence of dark and UV light conditions was investigated. Our results indicate that the removal percentage of adsorption in the dark is around 78% and in the light is about 90%. Adsorption behaviors of the Cu_2ONPs adsorbent fit well with pseudo-second-order kinetic model and Langmuir isotherm. The Cu_2ONPs were also found to be highly selective for anionic RR2 over cationic methylene blue dye, allowing facile separation of the two dyes from aqueous solutions of dye mixtures. The results also show that Cu_2ONPs have good recyclability, indicating that they would be a cost-effective material with a considerable possibility in water treatment.

Graphical abstract

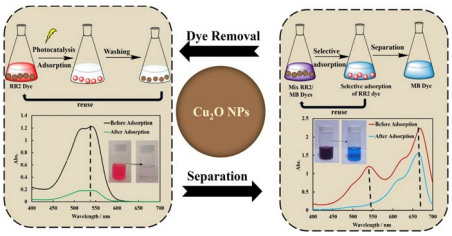

Keywords Adsorption · Photodegradation · Selective removal · Anionic dye · Cu_2ONPs

Introduction

Industrial pollution is a serious problem that has a negative impact on the environment. Water pollution containing dyes produced by companies and utilities is one of these forms of pollution [1]. The discharge of dangerous substances into the environment, such as heavy metals, pathogens and dyes is becoming a major global problem [2]. Synthetic dyes are

✉ Ahmed F. Halbus
ahmed.halbus@uobabylon.edu.iq

[1] Department of Chemistry, College of Science, University of Babylon, Hilla, Iraq

[2] Environmental Research and Studies Center, University of Babylon, Hilla, Iraq

used in different filed including packaging, paper, printing, food, textiles, leather, and pharmaceutical [3, 4]. Aromatic rings and azo groups with the propensity to create poisonous amines are the most common components of these dyes [3]. Dyes have unique qualities like high water solubility, high light stability, which can interfere with sunlight transmission into the water, carcinogenic, mutagenic, and poisonous impacts [5]. Thus, the removal of dyes from water and wastewater is a major global concern for human health and environmental protection [6, 7]. To date, coagulation [8], membrane separation [9], photocatalysis [10], and adsorption [11] have all been investigated as methods for removing dyes from water. Because of its simplicity and cheap cost, adsorption technology is regarded as one of the best efficient and cost-effective [12, 13]. For dyes removal, a variety of adsorbents have been utilized, including biomass materials, porous structure materials, metals and metal oxides [14–17]. To remove dye pollutions in practical applications, it is still necessary to investigate novel adsorbents with high efficiency [18]. Due to their porous nature and large specific surface area, metal oxide nanoparticles as adsorbents have gotten a lot of interest in recent years for removing synthetic dyestuffs from aqueous solutions via adsorption [19, 20]. Solar light is used in photocatalysis to generate hydrogen from water splitting, which then destroys organic contaminants. During photocatalysis, semiconductors absorb light energy that is more than or equal to their band gap, generating holes and electrons, which produce free radicals that oxidize the substrate [21]. Cuprous oxide is a p-type semiconductor with a 2.4 eV band gap [22]. Because of its interesting magnetic properties and unique optical [23] it becomes a promising material for a variety of uses like solar energy transformation [24–26]. It's also commonly utilized in gas sensors [27]. It's also a key component of co-oxidation [28] and is frequently utilized in lithium-ion batteries [29] and semiconductor technologies [30]. Cu_2ONPs are also appealing materials because of their low manufacturing costs and the natural availability of their precursor [31]. Photocatalysis is now one of the most widely used technologies for removing dyes and heavy metals from aqueous solutions [32–34]. This study aims to synthesize Cu_2O nanoparticles using direct precipitation and characterized. Cu_2ONPs were produced and employed as an adsorbent to remove anionic dyes. Cu_2O nanoparticles successfully removed the RR2 dye from an aqueous solution in a short period of time. We also report here the use of Cu_2ONPs, for the separation and selective adsorption of anionic RR2 dye from dye mixtures. Despite the ubiquity of Cu_2ONPs, there have been very few reports on selective dye separation, and no reports on the use of Cu_2ONPs for RR2 dye removal. Figure 1 shows a schematic of RR2 adsorption, selective removal and photocatalytic decolourisation on Cu_2ONPs in the existence of light and dark conditions.

Results and discussion

Characterization of the prepared Cu_2ONPs

The optimal conditions for Cu_2ONPs stability were determined by measuring zeta potential and particle size in aqueous solutions. At pH levels ranging from 3 to 12, the zeta potential (ZP) and particle size of this sort of sample were determined. Figure 2A displays the zeta potential measurements of produced Cu_2ONPs vs. different pH values. The zeta potential of Cu_2ONPs was about $+22 \pm 5$ mV and their average particles size was 147 ± 8 nm at pH 5, as displayed in Fig. 2B–D.

Figure 3A illustrates the XRD patterns of four samples of Cu_2ONPs that were synthesized without annealing and those that were annealed for 180 min at 100, 200, and 300 °C. Figure 3A shows that the peaks at 29.5°, 36.4°, 42.3°, 61.3°, 73.5°, 77.3° correspond to the Cu_2ONPs planes (110), (111), (200), (220), (311), and (222), respectively. There were no impurities and all diffraction peaks may be attributed to the pure shape of cubic Cu_2ONPs (cuprite—03-065-3288). The size of crystallite may be calculated by scherrer's formula $D = k\,\lambda/\beta\cos\theta$ where the constant k is taken to be 0.94, λ is the wavelength of X-ray, and β and θ are half width of peak and half of the Bragg angle, respectively. The data in Fig. 3B shows that the crystallite sizes were discovered to be about 22–34 nm. Figure 3C, D show SEM images of the synthesized Cu_2O nanoparticles. Using the Image J program, 200 particles were randomly selected from SEM images, the size of Cu_2ONPs was determined to be 62.84 ± 11 nm. Cu_2O nanoparticles have a cubic shape, which can be seen clearly in these images with the higher magnification (Fig. 3C) and is perfectly consistent with XRD analysis.

Figure 4 shows the FT-IR spectra in the region 500–4000 cm^{-1} that was obtained using four samples of Cu_2ONPs that had not been annealed and had been annealed at 100, 200, and 300 °C. Mostly, metals oxides have absorption bands under 1000 cm^{-1} because of interatomic vibrations [35]. In the FT-IR spectra of all four Cu_2ONPs studied, there was a strong peak appearing at about 535 cm^{-1}. The Cu–O stretching band corresponds to these emerging peaks. Nevertheless, there are discrepancies between the four samples in the asymmetric and symmetric frequencies between 1000 and 4000 cm^{-1}, which might be related to temperature's effect on the bands.

Adsorption and photocatalytic studies

The ability of the synthesized Cu_2ONPs to remove RR2 dye was tested. As shown in Fig. 4B, increasing the

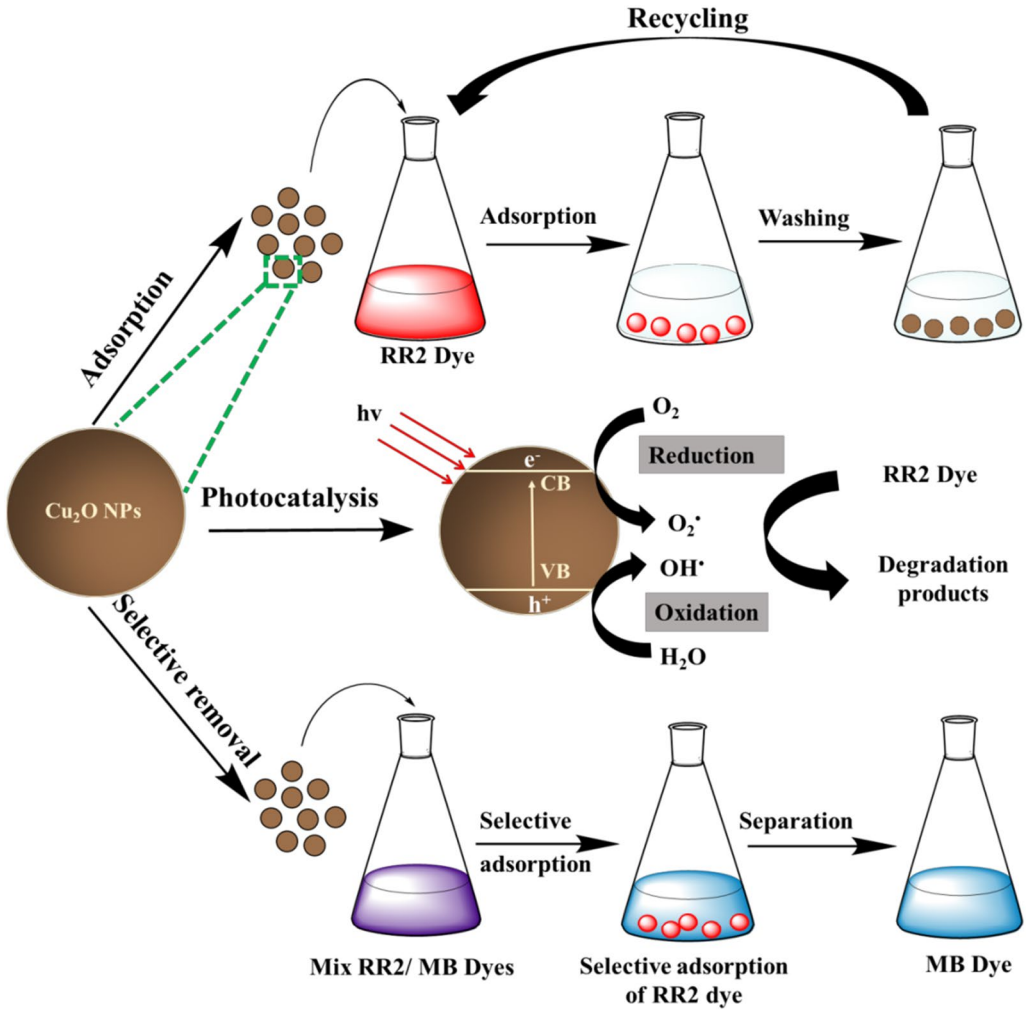

Fig. 1 Schematic diagram showing the photocatalytic process, selective removal and adsorption of Cu_2ONPs with RR2 dye in the existence of light and dark conditions

Cu_2ONPs dose resulted in an increase in RR2 dye adsorption percentage. This was attributed to the increased likelihood of the RR2 dye getting into contact with the available active sites of the Cu_2ONPs, which increases as the amount of adsorbent increases. Nevertheless, the RR2 dye adsorption capacity decreased as the Cu_2ONPs dose increased, as presented in Fig. 4B. This is due to the fact that the capacity of adsorption is inversely proportional to the amount of adsorbent used. In the current study, the efficiency of nanoparticles to remove RR2 dyes in dark and light conditions was assessed using RR2 dye as an anionic dye model. The UV–Vis spectra were used to determine the RR2 dye concentrations before and after adsorption under light and dark conditions, as presented in Fig. 5A, B. The RR2 dye was removed from the aqueous solution and adsorption of RR2 on the nanoparticles was observed. After adsorption, UV–Vis spectra reveal minimal absorption bands for RR2 dye in the solution. This effect might be explained by the electrostatic attraction between cationic Cu_2O nanoparticles and anionic dye, which causes the dye to be captured on nanoparticles. Due to the photoactivity of the nanoparticles, there was a significant difference in dye removal under dark (Fig. 5A) and UV light conditions (Fig. 5B) after adsorption of 0.1 g of Cu_2ONPs with 60 µg cm^{-3} of RR2 dye. Figure 5B also displays that the red solutions containing RR2 dye become very light, virtually clear and transparent after mixing the nanoparticles with RR2 dyes solutions for 3 h.

Furthermore, a batch adsorption approach was applied to investigate the adsorption behavior of Cu_2ONPs towards RR2 dye. At a pH 5, batch adsorption of RR2 dye was studied using 60 µg cm^{-3} of RR2 with a constant dose of nanoparticles (0.1 g) at various adsorption times. The adsorption of RR2 dye onto nanoparticles advanced quickly in the beginning, but the adsorption rate reduced gradually, reaching equilibrium after 40 min in the dark

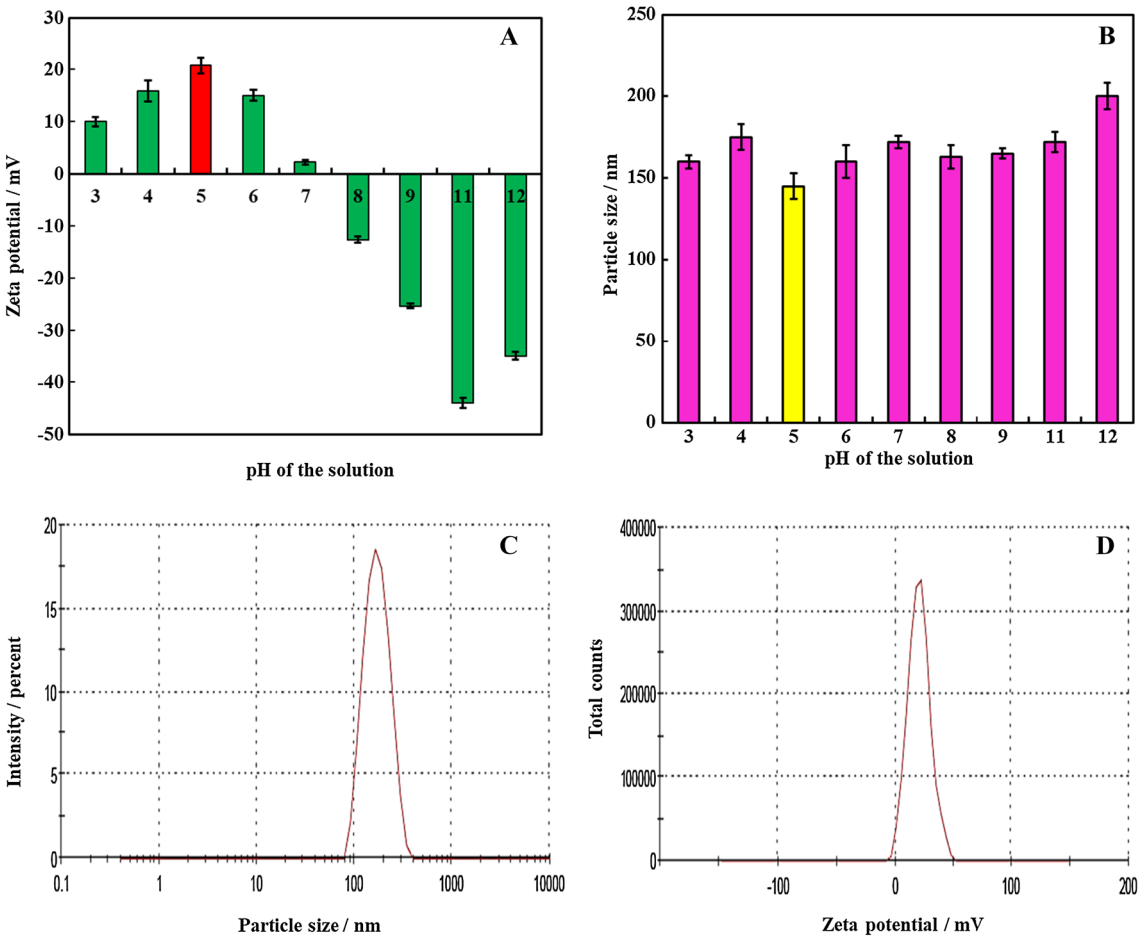

Fig. 2 **A** The zeta potential of the synthesized Cu_2ONPs solutions versus varied pH values. **B** The particle size of produced Cu_2ONPs at various pH. **C** The particle size and **D** zeta potential of Cu_2ONPs at pH 5

and 60 min under UV light, as shown in Fig. 6A. Because all of the adsorbent sites are initially unoccupied, the rate of adsorption changes quickly. After a period of time, the adsorption rate is low due to the diminish in the number of vacant adsorbent sites and the dye concentration. The lower rate of adsorption shows the probable monolayer creation of RR2 on the surface of adsorbent. As a result, after reaching equilibrium, the shortage of accessible active sites necessitates additional uptake [36]. In both light and dark conditions, the adsorption percentage of RR2 dye by nanoparticles was revealed. The rate of adsorption was sluggish in the dark, with around 78% RR2 dye eliminated after 3 h, but it was nearly 90% in the light. In the literature review, the decolourisation of dyes is familiar. The hydroxyl radicals (OH) are formed in a reaction that functions as oxidant, which is deposited on Cu_2ONPs. The hydroxyl ion radicals are formed when water molecules on the surface of nanoparticles react with holes ($h+_{(VB)}$). Thus, the RR2 dye is degraded by hydroxyl ion radicals [37–39].

Kinetics of RR2 dye adsorption

Kinetic studies are extremely important in the adsorption field because they give insight into the adsorption mechanism. A substance that will be employed as an adsorbent must have a higher adsorption ability and rate constant. Pseudo first- [40] and second-order [41] kinetics were applied in this study. Figure 6B–D illustrate the matching plots of the kinetic model of adsorption. Figure 6B shows first-order reaction kinetic plots for RR2 dye, whereas Fig. 6C shows second-order reaction kinetic plots for RR2 dye. The pseudo-second-order model's correlation coefficient was found to be much greater than the pseudo-first-order model's (Table 1). Moreover, the simulated adsorption capacity obtained from the plot of the pseudo-second-order model was found to be better matched to the actual data than that calculated from the pseudo-first order model (see Fig. 6B, C). The adsorption mechanism for RR2 dye on nanoparticles is thus best defined by the pseudo-second-order model. Therefore, an intraparticle diffusion model [42] was

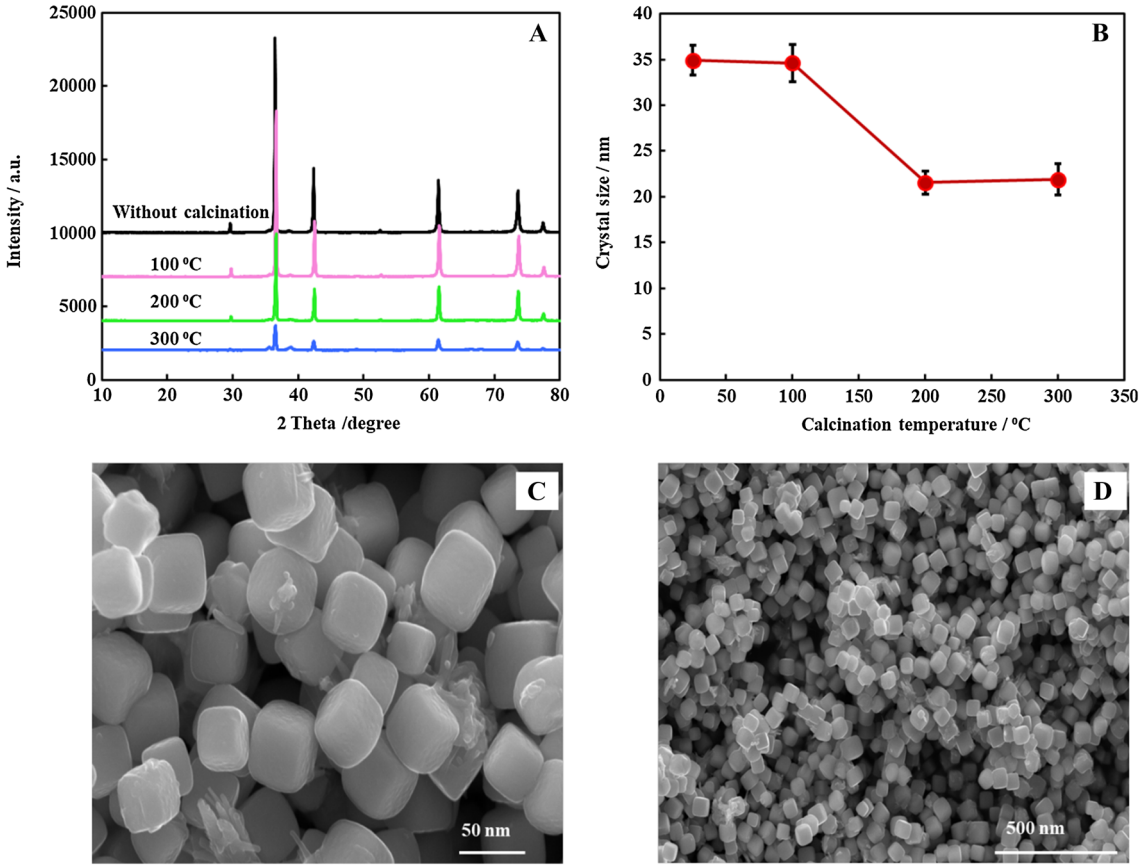

Fig. 3 **A** XRD pattern of as-prepared nanosized Cu_2O at different calcination temperatures. **B** The effect of calcination temperature on crystal size of Cu_2ONPs. **C**, **D** SEM images of as-prepared nanosized Cu_2O at different magnifications

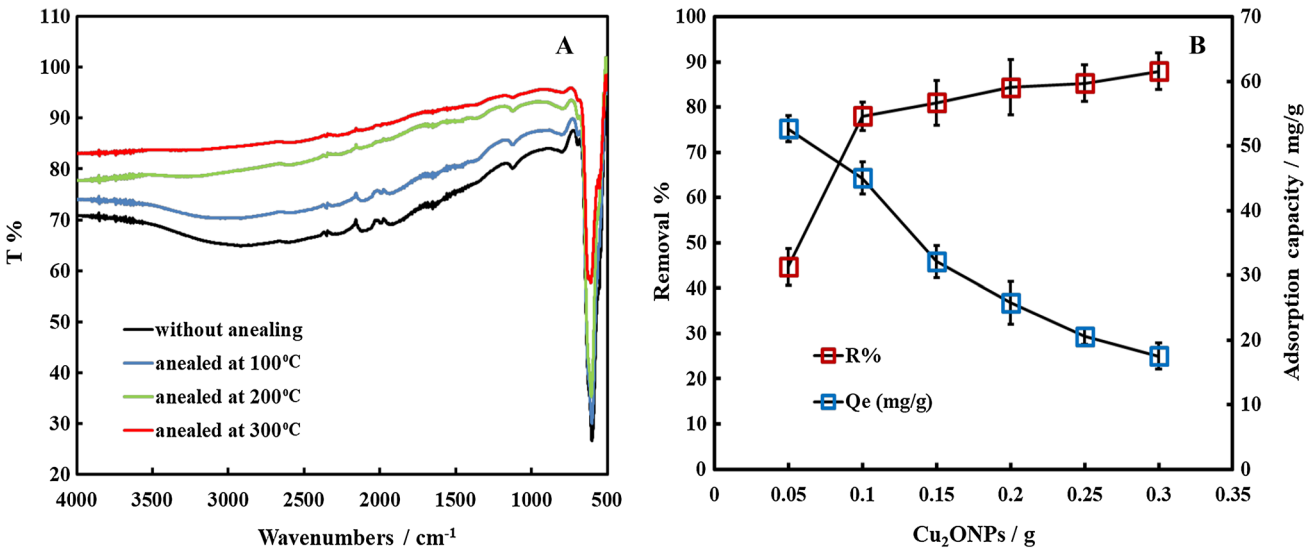

Fig. 4 **A** The FT-IR spectra of the created Cu_2ONPs before and after calcination. **B** The effect of Cu_2ONPs mass on the removal percentage (R%) and adsorption capacity of RR2 dye

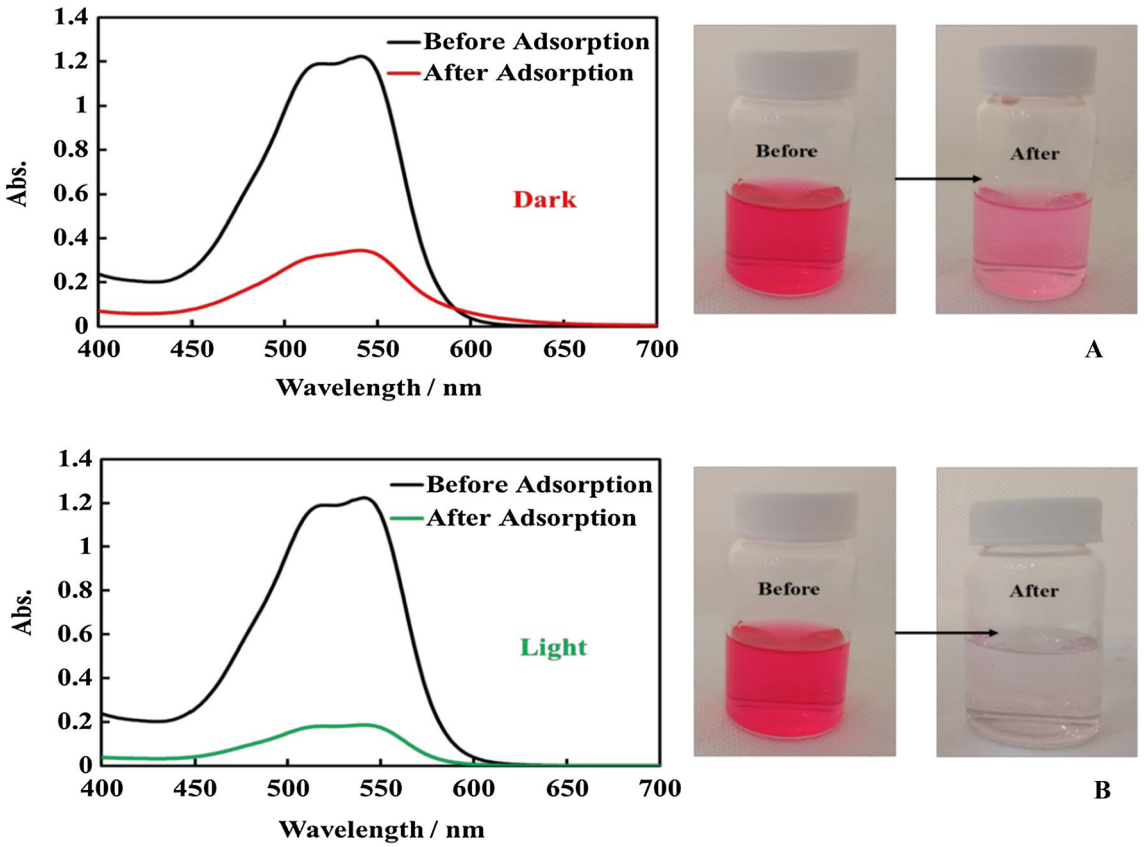

Fig. 5 UV–Vis spectra of RR2 **A** in dark and **B** UV light before and after adsorption using Cu_2ONPs for 3 h. Insets are the images of RR2 dye solutions before and after adsorption for 3 h

used to demonstrate how RR2 molecules moved from the solution to the Cu_2ONPs interconnecting pores. The linear plot for RR2 dye does not pass through the origin, showing that the intraparticle diffusion models are based on the migration of adsorbates into nanoparticles and controlling the rate adsorption process, as shown in Fig. 6D. The adsorbent parameters data for the intraparticle diffusion model are scheduled in Table 1 for RR2 dye.

Adsorption isotherms

The isotherm models provide useful information for predicting the interaction of adsorbate particles and adsorbents. The mechanism of RR2 dye adsorption onto Cu_2ONPs was explored by examining the adsorption characteristics using the Langmuir and Freundlich linear isotherm models. The Langmuir isotherms of RR2 dye are shown in Fig. 7A, while the Freundlich isotherm models are shown in Fig. 7B. The maximum adsorption capacities of RR2 dye molecules for the synthesized nanoparticles were calculated using these models. The results from the RR2 dye adsorption experiments match well with the Langmuir isotherm model, according to these isotherms. The maximal adsorption capacities of RR2 dye are calculated to be 64.102 mg g^{-1} based on the Langmuir isotherm model at pH 5, 60 µg cm^{-3} RR2 concentration, 0.1 g of Cu_2ONPs and 25 °C (Fig. 7A, B). To show the heterogeneities on the surface of Cu_2ONPs, the Freundlich model's computed n values are utilized (Fig. 7C). Adsorption will be physical for n more than 1, linear for *n* equal 1, and chemical for n less than 1. In this work, the RR2 dye has *n* more than 1 value, suggesting physical absorption [43, 44].

Separation of a mixture of dyes

Cu_2ONPs was used to selectively separate various organic dyes due to their unique and rapid adsorption activity towards RR2 dye. RR2/MB dye mixtures in an aqueous solution with varied charge states were used to test the separation performance of Cu_2ONPs. Cu_2ONPs are intended to remove RR2 dye with a negative charge from the mixed solution, whereas MB dye with a positive charge should be left in the solution. The colors of the dye combination of RR2 and MB before and after adsorption with Cu_2ONPs were captured by digital images, as shown in Fig. 8B–E, and Cu_2ONPs were compared to those of the two individual aqueous solutions

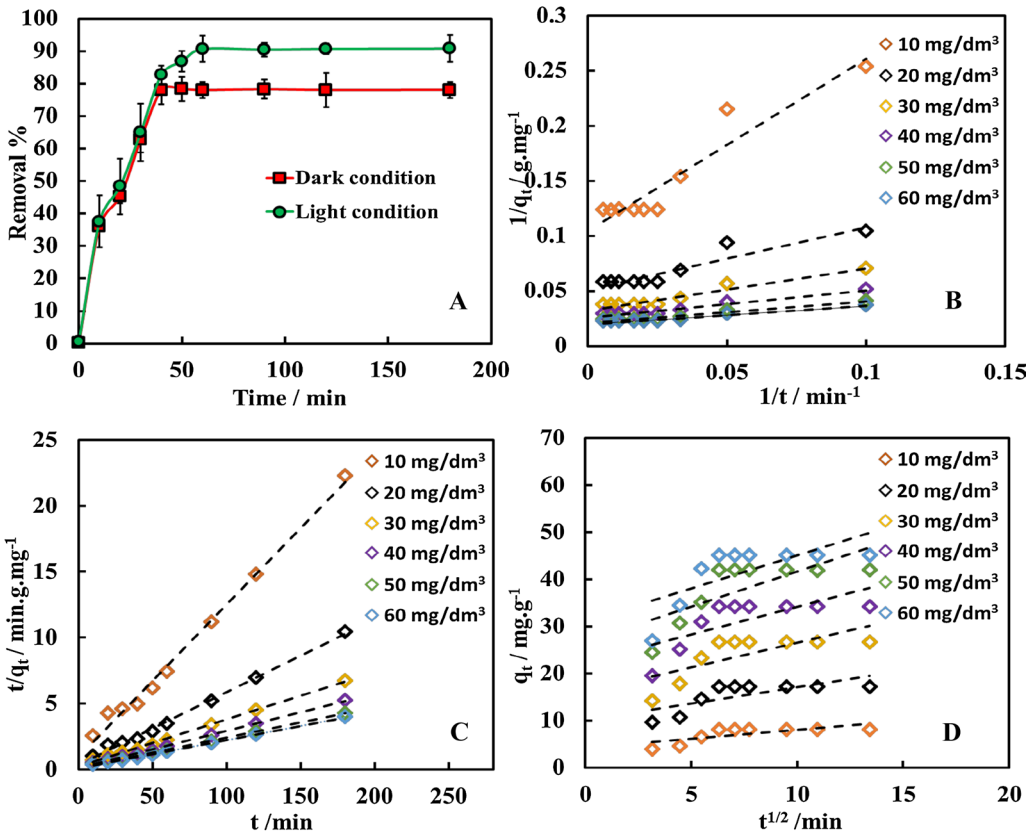

Fig. 6 **A** The influence of time on the removal percentage of RR2 dye in dark and light conditions (the initial RR2 concentration: 60 µg cm^{-3}, adsorbent dosage: 0.1 g in 100 cm^3 of RR2 solutions, shaking rate is constant at 100 rpm, t = 25 °C, pH = 5). Kinetic models for the adsorption of RR2 dye with Cu_2ONPs **B** pseudo-first order model for RR2 dye and **C** pseudo-second order model and **D** intraparticle diffusion model for RR2 dye

Table 1 Pseudo first, pseudo second order kinetic and intraparticle diffusion models for adsorption of RR2 on Cu_2ONPs

C_0/mg dm^{-3}	Pseudo-first order kinetic model				Pseudo-second order kinetic model			Intraparticale diffusion model		
	$q_{e,exp}$/mg g^{-1}	$q_{e,cal}$/mg g^{-1}	k_1/min^{-1}	R^2	$q_{e,cal}$/mg g^{-1}	k_2/g mg^{-1} min^{-1}	R^2	C/mg g^{-1}	kp/mg g^{-1} $min^{-1/2}$	R^2
10	8.078	9.551	12.641	0.901	8.643	0.1262	0.992	4.188	0.380	0.554
20	17.263	19.493	9.745	0.876	18.181	0.1591	0.995	10.048	0.703	0.543
30	26.677	30.864	10.126	0.938	28.011	0.177	0.996	15.973	1.053	0.533
40	34.234	38.910	8.524	0.950	35.587	0.226	0.998	22.321	1.177	0.516
50	41.954	47.393	8.218	0.946	43.478	0.231	0.998	26.709	1.492	0.555
60	45.114	50.761	7.579	0.945	46.511	0.268	0.998	26.955	2.077	0.612

of RR2/MB dyes. After combining RR2 and MB dyes, the color of the combination of red RR2 (Fig. 8B) and blue MB (Fig. 8C) turned purple (Fig. 8D). After 3 h of adsorption, practically all of the RR2 dye was caught by the Cu_2ONPs, and the color of the dye combination solution changed from purple to blue (Fig. 8E), matching the color of the pure MB aqueous solution. UV–Vis spectra were used to measure the concentrations of RR2 and MB in the mix solution before and after 3 h of adsorption with Cu_2ONPs, as shown in Fig. 8A. After 3 h, UV–Vis spectra show that approximately 98% RR2 was adsorbed by Cu_2ONPs, on the other hand only 20% MB was adsorbed. This shows that Cu_2ONPs selectively adsorb RR2 from the dye mixture, allowing the dye mixture to be separated successfully. These results could be described by the lower adsorption of the Cu_2ONPs to the MB dye, due to electrostatic repulsion and the improved particle-dye adsorption because of electrostatic interaction in the situation of cationic Cu_2ONPs with anionic RR2 dye.

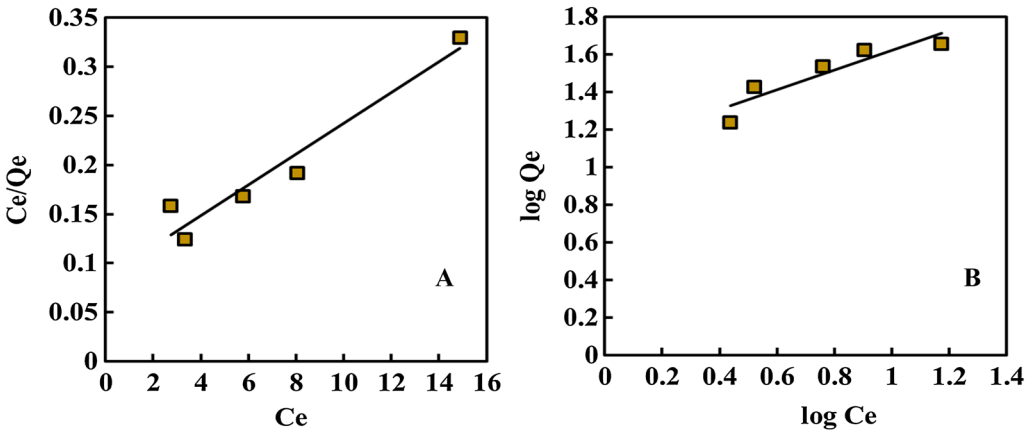

C

Langmuir			Freundlich		
q_m / mg.g^{-1}	b / dm^3.g^{-1}	R^2	K_f/ mg.g^{-1}	n	R^2
64.102	0.181	0.934	12.548	1.916	0.839

Fig. 7 **A** Adsorption isotherms for RR2 dye on Cu_2ONPs according to Langmuir. **B** Adsorption isotherms for RR2 on Cu_2ONPs according to Freundlich. **C** Constants of Freundlich and Langmuir isotherms

Regeneration and reuse of used Cu_2ONPs

The sustainable reuse of an adsorbent is actually essential in workable applications. Therefore, the regeneration and reuse of the used Cu_2ONPs was also evaluated for 5 cycles adsorption/desorption and the data are presented in Fig. 9. The desorption of RR2 was applied by immersing the loaded RR2- Cu_2ONPs in 0.01 N NaOH for 3 h followed by washing with DW. As expected the deprotonation makes decreases electrostatic attraction between the Cu_2ONPs and the negatively charged dye. After five cycles of adsorption–desorption, Cu_2ONPs exhibit a high removal efficiency. The RR2 dye removal efficiency decreased as the number of reuse cycles increased; however, the Cu_2ONPs loosed only 9% of its original efficiency during the five cycles. The decrease in removal efficiency might thus be a result of the alteration of the Cu_2ONPs surface properties during the adsorption–desorption processes [45]. These findings show that Cu_2ONPs have high recyclability, making them a cost-effective material with a good possibility in water treatment.

Conclusions

In this paper, we describe the synthesis and characterization of Cu_2ONPs using SEM, FT-IR, DLS, and XRD analysis techniques. DLS analysis data displayed that the zeta potential of Cu_2ONPs was measured to be $+22 \pm 5$ mV with a hydrodynamic diameter of 147 ± 8 nm at pH 5 which was the most suitable medium for the particles to be at higher stability. However, using the Image J program and randomly chosen 200 particles from SEM images, the average size of Cu_2ONPs was determined to be 62.84 ± 11 nm. Cu_2ONPs with a nano-sized diameter and homogenous cubic shape were synthesized successfully, according to SEM images. The results from XRD and FTIR analysis also confirmed that Cu_2ONPs were synthesized successfully. The adsorption of RR2 dye onto Cu_2ONPs and its photocatalytic activity were then studied. The removal percentage of RR2 dye adsorption on Cu_2ONPs was determined to be about 78% in dark conditions while RR2 dye degrades by 90% when exposed to UV light in the presence Cu_2ONPs. The kinetics of RR2 dye adsorption were examined to evaluate the adsorption process, and the findings revealed that the kinetic data acceptable the pseudo-second-order kinetic model effectively. The adsorption equilibrium results for RR2 dye adsorption were also discovered to greatest suitable the Langmuir isotherm model. It was also discovered that the anionic dye has much higher adsorbed selectively on the Cu_2ONPs adsorbent than the cationic ones. The results also confirm that Cu_2ONPs exhibited great recyclability performance and thus they will be cost-effective material and have excellent possible in water treatment.

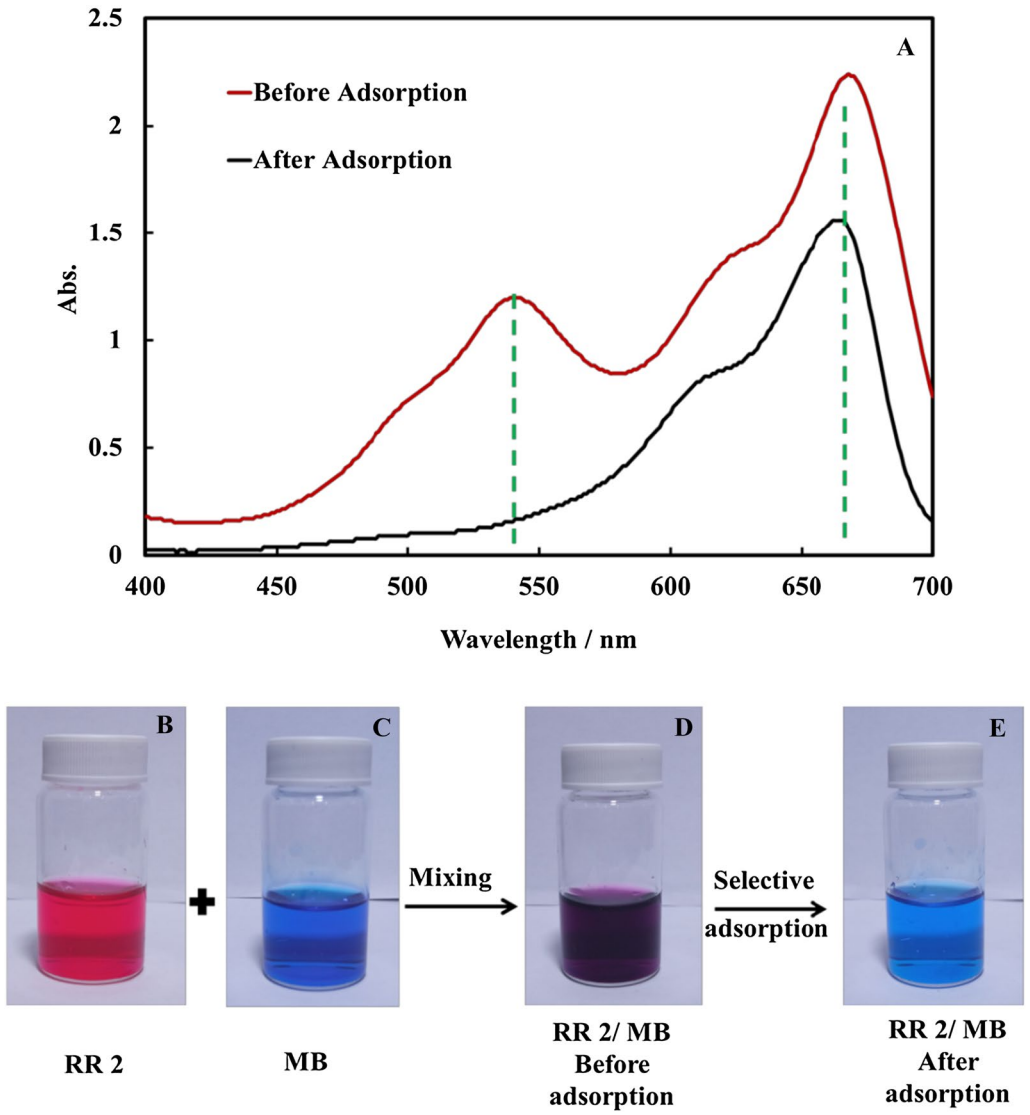

Fig. 8 **A** UV–Vis spectra of RR2/MB mixture solutions before and after adsorption on the Cu_2ONPs adsorbent. **B** Photos of the RR2 dye; **C** photos of the MB dye; **D** photos of the RR2/MB mixture solutions before adsorption and **E** after adsorption

Experimental

Cuprous oxide nanoparticles were synthesized using cupric chloride, sodium hydroxide, and ascorbic acid, all of these chemicals were provided from Sigma-Aldrich, UK. RR2 dye was provided via Ciba company, Switzerland and used for this work without any additional purification.

Method

Cuprous oxide nanoparticles can be prepared in a variety of methods. These methods are dependent on the conditions of the reaction like reducing agents and temperature as well as the sources of copper atoms. Direct precipitation of Cu_2ONPs is one of the most used methods. Briefly, the experiment includes the reaction of sodium hydroxide with cupric chloride in the existence of ascorbic acid as a reducing agent. The experimental procedure in this study began with the preparation of three stock solutions of 0.05 M cupric chloride, 0.113 M sodium hydroxide, and 0.009 M ascorbic acid by dissolving 0.7596 g of cupric chloride, 0.4520 g of sodium hydroxide, and 0.1585 g of ascorbic acid in Milli-Q water using three of 100 cm^3 volumetric flasks, respectively. Cu_2ONPs were produced by gently mixing 16 cm^3 of 0.113 M sodium hydroxide solution with 16 cm^3 of 0.05 M cupric chloride solution in a 100 cm^3 beaker at 500 rpm after the stock solution stage was completed. After the color of the solution had darkened to a thick dark blue, 10 cm^3 of 0.009 M ascorbic acid was added to the solution and stirred continuously for 30 min. During this time, the solution color

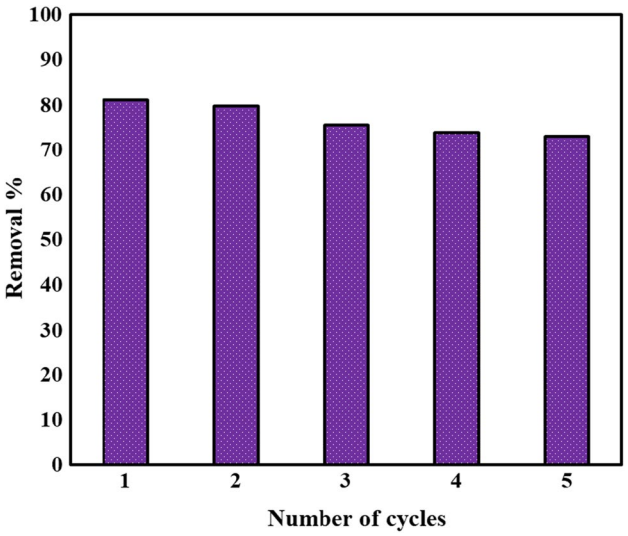

Fig. 9 Reusability of Cu_2ONPs for the removal of RR2 dye

changed rapidly from dark blue to green, then stabilized with the appearance of turbid red, indicating the production of Cu_2ONPs. The stirring was then halted, and the precipitate was covered with aluminum foil to avoid oxidation by air, and allowed to settle for about 60 min. This was followed by collecting the precipitate, which was centrifuged for 60 min at 5000 rpm. The sediment was then collected and dispersed in Milli-Q water using a shaking machine after the turbid supernatant was discarded. After that, the washing procedure and centrifugation of dispersed Cu_2ONPs were repeated five times. All of these procedures were performed at room temperature. Lastly, the nanoparticles were dried at 50–70 °C in a drying oven [46]. The formed nanoparticles were weighed and calcined in the furnace for 180 min at three various temperatures 100 °C, 200 °C, and 300 °C under nitrogen, all these nanoparticles were kept away from exposure to O_2 using vials with tight lids.

Adsorption and photocatalytic experiments

RR2 was chosen to study the capacity of adsorption of the Cu_2ONPs. The experimental findings were registered with a UV–Vis spectrophotometer set to 541 nm. Cu_2ONPs were produced and added to 100 cm^3 of RR2 dye solutions. A platform shaker was used to shake the solutions on a regular basis for 3 h in the dark condition. Before and after adsorption, we examined the absorbance at the maximum absorption wavelength. The removal percentage (R %) of RR2 dye on Cu_2ONPs was determined via batch adsorption testing, which involved placing 0.1 g of Cu_2ONPs with 100 cm^3 serial solutions of 10–60 µg cm^{-3} of RR2 dye in separate conical flasks. At a shaker speed of 150 rpm, the Cu_2ONPs containing RR2 were nicely shaken at 25 ± 3 °C in the dark condition until they reached equilibrium. The concentration of RR2 dye was assessed using UV–Vis spectrophotometer (1650 PC-Shimadzu UV–Visible spectrometer). The RR2 removal percentage and the adsorption quantity of the dye adsorbed per unit mass of adsorbent at particular time Q_t and at equilibrium Q_e (mg g^{-1}) were calculated according to the following equations [47]:

$$\%R = \frac{C_0 - C_t}{C_0} \times 100\%$$

$$Q_t = \frac{(C_0 - C_t)V}{m}$$

$$Q_e = \frac{(C_0 - C_e)V}{m}$$

where C_0 is the initial concentration of RR2 (mg dm^{-3}) before adsorption, C_t is the RR2 concentration after adsorption at a given time t, C_e is the concentration of RR2 in solution at equilibrium time (mg dm^{-3}), V is the volume of RR2 solution (dm^3), and m is the weight of Cu_2ONPs (g).

In the presence of light, we also investigated the photodegradation activity of RR2 with Cu_2ONPs. The photocatalytic experiment was conducted in a photochemical reactor equipped with four 15 W mercury lamps from Philips (CLEO), Poland. A platform shaker was used to irradiate aqueous solutions of Cu_2ONPs with RR2 in conical flasks. The Cu_2ONPs were suspended in 100 cm^3 of an aqueous solution of RR2 in all of the tests. 4 cm^3 of the reaction suspension was taken after illumination and spun at 3,500 rpm in an 800 B centrifuge for 30 min. to extract the Cu_2ONPs. To remove tiny Cu_2O particles, second centrifugation was found to be essential. The RR2 absorbance was measured at 541 nm after the second centrifugation. The RR2 removal percentage was also calculated according to the above equation [48].

Acknowledgements Authors gratefully acknowledge the Department of Chemistry, College of Science, University of Babylon for providing research facilities to carry out this work.

References

1. Radwan NRE, El-Shall MS, Hassan HMA (2007) Appl Catal A 331:8
2. Evans S, Campbell C, Naidenko OV (2019) Heliyon 5:e02314
3. Masoudian N, Rajabi M, Ghaedi M (2019) Polyhedron 173:114105
4. Joshi S, Garg VK, Kataria N, Kadirvelu K (2019) Chemosphere 236:124280
5. Sartape AS, Mandhare AM, Jadhav VV, Raut PD, Anuse MA, Kolekar SS (2017) Arab J Chem 10:S3229
6. Hajati S, Ghaedi M, Mahmoudi Z, Sahraei R (2015) Spectrochim Acta Part A Mol Biomol Spectrosc 150:1002

7. Wu Y, Su M, Chen J, Xu Z, Tang J, Chang X, Chen D (2019) Dyes Pigm 170:107591
8. Fan M, Wang Y, Wang Z, Zhao Y, Gao B, Chu Y, Zhou W, Yan C (2019) J Clean Prod 238:117984
9. Zhan Y, Wan X, He S, Yang Q, He Y (2018) Chem Eng J 333:132
10. Li X, Shi J-L, Hao H, Lang X (2018) Appl Catal B Environ 232:260
11. Yousefi M, Villar-Rodil S, Paredes JI, Moshfegh AZ (2019) J Alloys Compd 809:151783
12. Zheng Y, Cheng B, You W, Yu J, Ho W (2019) J Hazard Mater 369:214
13. Wu Z, Zhang H, Luo L, Tu W (2019) J Alloys Compd 806:823
14. Jawad AH, Abdulhameed AS (2020) Surf Interfaces 18:100422
15. Jawad AH, Abdulhameed AS, Mastuli MS (2020) J Polym Environ 28:1095
16. Abdulhameed AS, Mohammad AT, Jawad AH (2019) Desalin Water Treat 164:346
17. Jawad AH, Abdulhameed AS, Mastuli MS (2020) J Taibah Univ Sci 14:305
18. Sun J, Song T, Wang J, Guo X, Su L, Tu W (2020) SN Appl Sci 2:1103
19. Sharma JK, Srivastava P, Singh G, Akhtar MS, Ameen S (2015) Thermochim Acta 614:110
20. Lansari I, Benguella B, Kruchinina N, Nistratov A (2022) React Kinet Mech Catal 135:987
21. Shinde DR, Tambade PS, Chaskar MG, Gadave KM (2017) Drink Water Eng Sci 10:109
22. Kumar RV, Mastai Y, Diamant Y, Gedanken A (2001) J Mater Chem 11:1209
23. Self K, Zhou W (2016) Cryst Growth Des 16:5377
24. Dai P, Mook HA, Aeppli G, Hayden SM, Doğan F (2000) Nature 406:965
25. Briskman RN (1992) Sol Energy Mater Sol Cells 27:361
26. Khan MA, Ullah M, Iqbal T, Mahmood H, Khan AA, Shafique M, Majid A, Ahmed A, Khan NA (2015) Nanosci Nanotechnol Res 3:16
27. Zhang J, Liu J, Peng Q, Wang X, Li Y (2006) Chem Mater 18:867
28. White B, Yin M, Hall A, Le D, Stolbov S, Rahman T, Turro N, O'Brien S (2006) Nano Lett 6:2095
29. Li J, Yu N, Geng H (2016) Phys Chem Chem Phys 18:21562
30. Liu R, Kulp EA, Oba F, Bohannan EW, Ernst F, Switzer JA (2005) Chem Mater 17:725
31. Liu YL, Liu YC, Mu R, Yang H, Shao CL, Zhang JY, Lu YM, Shen DZ, Fan XW (2004) Semicond Sci Technol 20:44
32. Kangralkar MV, Kangralkar VA, Momin N, Manjanna J (2019) Env Nanotechnol Monit Manag 12:100265
33. Riyat M, Islam R, Salam A, Molla M, Hossain T, Islam M, Bashar M, Chandra D, Ahsan S, Roy D, Ahsan M (2022) React Kinet Mech Catal 135:1077
34. Zhang H, Duan C, Xu Z, Yin J (2022) React Kinet Mech Catal 135:1099
35. Topnani N, Kushwaha S, Athar T (2010) Int J Green Nanotechnol Mater Sci Eng 1:M67
36. Bellir K, Bencheikh-Lehocine M, Meniai AH (2010) Int Renew Energy Congr 2010:360
37. Hussein FH, Halbus AF, Hassan HAK, Hussein WAK (2010) E-Journal Chem 7:540
38. Kamil AM, Hussein FH, Halbus AF, Bahnemann DW (2014) Int J Photoenergy 2014:475713
39. Ahmed LM, Alkaim AF, Halbus AF, Hussein FH (2016) Int J ChemTech Res 9:90
40. Lagergren S (1898) Handlingar 24:1
41. Ho Y-S, McKay G (1999) Process Biochem 34:451
42. Zhou C, Wu Q, Lei T, Negulescu II (2014) Chem Eng J 251:17
43. Fawzy MA, Gomaa M (2021) J Appl Phycol 33:675
44. Bhavyasree PG, Xavier TS (2021) Curr Res Green Sustain Chem 4:100161
45. Rathinam K, Kou X, Hobby R, Panglisch S (2021) Mater 14:7701
46. Cao Y, Xu Y, Hao H, Zhang G (2014) Mater Lett 114:88
47. Halbus AF, Lafta AJ, Athab ZH, Hussein FH (2014) Asian J Chem 26:S167
48. Hussein FH, Halbus AF (2012) Int J Photoenergy 2012:495435